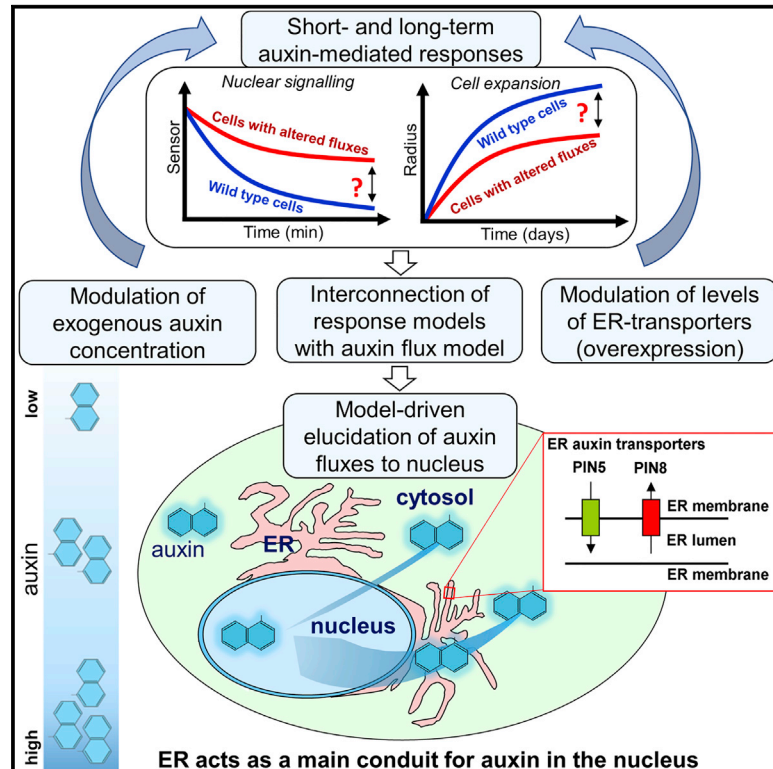


## Data-Driven Modeling of Intracellular Auxin Fluxes Indicates a Dominant Role of the ER in Controlling Nuclear Auxin Uptake

### Graphical Abstract



### Authors

Alistair M. Middleton, Cristina Dal Bosco, Phillip Chlap, ..., Klaus Palme, Christian Fleck, Alexander Dovzhenko

### Correspondence

klaus.palme@biologie.uni-freiburg.de (K.P.), christian.fleck@wur.nl (C.F.), alexander.dovzhenko@biologie.uni-freiburg.de (A.D.)

### In Brief

Middleton et al. study how the plant phytohormone auxin enters the nucleus by using quantitative phenotyping in single plant cell systems and bespoke mathematical models that relate controlled perturbations to experimentally measurable responses. Their findings show that auxin predominantly enters the nucleus via the endoplasmic reticulum.

### Highlights

- Auxin transport probe NBD-NAA does not enter the nucleus by simple diffusion
- Modulation of auxin transport at the ER affects auxin-mediated responses
- Model of nuclear auxin fluxes interconnects short- and long-term auxin responses
- The ER is the main conduit for nuclear auxin uptake



# Data-Driven Modeling of Intracellular Auxin Fluxes Indicates a Dominant Role of the ER in Controlling Nuclear Auxin Uptake

Alistair M. Middleton,<sup>1,8,12</sup> Cristina Dal Bosco,<sup>2,12</sup> Phillip Chlap,<sup>3,10</sup> Robert Bensch,<sup>3,5</sup> Hartmann Harz,<sup>4</sup> Fugang Ren,<sup>2</sup> Stefan Bergmann,<sup>2</sup> Sabrina Wend,<sup>2</sup> Wilfried Weber,<sup>2,5</sup> Ken-ichiro Hayashi,<sup>7</sup> Matias D. Zurbriggen,<sup>2,5,6</sup> Rainer Uhl,<sup>4</sup> Olaf Ronneberger,<sup>3,5</sup> Klaus Palme,<sup>2,5,8,9,13,\*</sup> Christian Fleck,<sup>9,11,13,\*</sup> and Alexander Dovzhenko<sup>2,13,14,\*</sup>

<sup>1</sup>Centre for Modeling and Simulation in the Biosciences, University of Heidelberg, 69120 Heidelberg, Germany

<sup>2</sup>Institute of Biology II, University of Freiburg, 79104 Freiburg, Germany

<sup>3</sup>Institute of Computer Science, University of Freiburg, 79110 Freiburg, Germany

<sup>4</sup>Biolmaging Center, University of Munich, 82152 Martinsried, Germany

<sup>5</sup>BIOS Centre for Biological Signalling Studies, University of Freiburg, 79104 Freiburg, Germany

<sup>6</sup>Institute of Synthetic Biology, University of Düsseldorf, 40225 Düsseldorf, Germany

<sup>7</sup>Department of Biochemistry, University of Okayama, 700-0005 Okayama, Japan

<sup>8</sup>Freiburg Institute for Advanced Sciences (FRIAS), University of Freiburg, 79104 Freiburg, Germany

<sup>9</sup>Centre for Biological Systems Analysis (ZBSA), University of Freiburg, 79104 Freiburg, Germany

<sup>10</sup>Present address: Faculty of Computer Science, Multimedia Information Systems, University of Vienna, 1090 Vienna, Austria

<sup>11</sup>Present address: Systems and Synthetic Biology, Wageningen University, 6703 Wageningen, the Netherlands

<sup>12</sup>These authors contributed equally

<sup>13</sup>Senior author

<sup>14</sup>Lead Contact

\*Correspondence: [klaus.palme@biologie.uni-freiburg.de](mailto:klaus.palme@biologie.uni-freiburg.de) (K.P.), [christian.fleck@wur.nl](mailto:christian.fleck@wur.nl) (C.F.), [alexander.dovzhenko@biologie.uni-freiburg.de](mailto:alexander.dovzhenko@biologie.uni-freiburg.de) (A.D.)

<https://doi.org/10.1016/j.celrep.2018.02.074>

## SUMMARY

In plants, the phytohormone auxin acts as a master regulator of developmental processes and environmental responses. The best characterized process in the auxin regulatory network occurs at the subcellular scale, wherein auxin mediates signal transduction into transcriptional programs by triggering the degradation of Aux/IAA transcriptional repressor proteins in the nucleus. However, whether and how auxin movement between the nucleus and the surrounding compartments is regulated remain elusive. Using a fluorescent auxin analog, we show that its diffusion into the nucleus is restricted. By combining mathematical modeling with time course assays on auxin-mediated nuclear signaling and quantitative phenotyping in single plant cell systems, we show that ER-to-nucleus auxin flux represents a major subcellular pathway to directly control nuclear auxin levels. Our findings propose that the homeostatically regulated auxin pool in the ER and ER-to-nucleus auxin fluxes underpin auxin-mediated downstream responses in plant cells.

## INTRODUCTION

The plant hormone auxin, while structurally simple, is known to regulate a multitude of processes in plants—from embryo

patterning and development to *de novo* organ formation and environmental responses (Freire Rios et al., 2014; Wu et al., 2015; Naseem et al., 2015; Taylor-Teeple et al., 2016). Although it is not yet completely understood how auxin can orchestrate such an astonishing range of processes, there has been significant progress in our comprehension of auxin perception and signal transduction.

The best characterized pathway for auxin signaling involves the regulation of genes at the transcriptional level. The current accepted model of auxin-mediated transcriptional responses considers the interplay between auxin and nuclear receptors F-box TIR1/AFBs, transcriptional repressors Aux/IAA, and transcriptional factors ARFs, with 6, 29, and 23 members identified in *Arabidopsis thaliana*, respectively (Salehin et al., 2015). At elevated nuclear auxin levels, Aux/IAs and TIR1/AFBs form co-receptor complexes in an auxin-dependent manner. Following complex formation, Aux/IAs are ubiquitinated and marked for proteolysis, thus releasing ARFs to drive the transcriptional responses (Dharmasiri et al., 2005; Kepinski and Leyser, 2005). The dynamic range of auxin is tuned by the combinatorial assembly of the various Aux/IAs with TIR1/AFBs, resulting in a series of co-receptors with different auxin binding affinities (Calderón Villalobos et al., 2012; Wang and Estelle, 2014). Upon taking into account the critical role of auxin levels in the assembly of the co-receptor complexes (Tan et al., 2007), key questions arise: How does auxin enter the nucleus? And is this process regulated?

The mechanisms underpinning nuclear auxin uptake remain unclear. As a small molecule, IAA (indole-3-acetic acid) could potentially enter the nucleus via diffusion through the nuclear



pores without restriction (Wei et al., 2003). However, it remains unclear whether this alone could account for the observed dynamics of auxin-regulated gene expression (Wang and Estelle, 2014) or whether a rate-limited mechanism or mechanisms might be involved.

Novel fluorescent auxin analogs have been developed that mimic native auxin transport and accumulation *in vivo* without affecting auxin signaling (Hayashi et al., 2014). These 7-nitro-2,1,3-benzoxadiazole (NBD)-conjugated synthetic auxin analogs allowed visualization of subcellular auxin transport and distribution, revealing their preferential accumulation in the endoplasmic reticulum (ER) of tobacco BY-2 and *Arabidopsis* root cells (Hayashi et al., 2014). Moreover, the ER-residing auxin transport proteins from the PIN and PILS families affect cellular auxin homeostasis and nuclear auxin signaling (Barbez et al., 2012; Dal Bosco et al., 2012; Ding et al., 2012; Mravec et al., 2009). The outer membrane of the nuclear envelope is continuous with the ER, such that the space between the inner and the outer nuclear membranes is directly connected with the lumen of the ER (Meier and Brkljacic, 2010). Altogether, we sought to disentangle the interplay among the ER, the cytosol, and the nucleus in relation to nuclear auxin uptake.

We developed a joint theoretical-experimental approach to unravel this puzzle by resolving two major challenges: the complex organization of the plant due to cellular heterogeneity and the need to quantitatively assess intracellular auxin transport dynamics. Auxin transport between subcellular compartments cannot be measured directly due to the lack of non-invasive methods and tools. Therefore, indirect time-resolved auxin dose responses in single plant cell systems at different scales were combined with modeling approaches. Data-driven mathematical models of intracellular auxin transport were specifically tailored to interpret nuclear auxin uptake. Analysis of the model results indicated a dominant role of ER-to-nucleus auxin fluxes in regulating nuclear auxin levels. Our finding suggests that ER auxin pool and ER-to-nucleus transport rates underpin auxin-mediated signaling responses in plant cells.

## RESULTS

### Concept of Nuclear Auxin Uptake Exploration

The fundamental idea behind our approach is to infer intracellular auxin fluxes, which cannot be evaluated directly, using bespoke models that relate controlled perturbations to experimentally measurable responses. It was therefore crucial to minimize the complexity of the plant system by using single plant cells (Figure 1A). As controlled perturbations, we modulated intracellular auxin fluxes by overexpressing ER-localized auxin transporters (Figure 1A) and developed assays to measure long-term and short-term responses at different auxin concentrations (Figure 1B). For long-term responses, we monitored expansion of single plant cells, whereas for short-term responses, we used an auxin sensor (Figure 1B). Models describing these responses were independently coupled to a model for the nuclear auxin fluxes (Figure 1C). The coupled models were fitted to the response data to generate estimates for various flux parameters among the nucleus, the ER, and the cytosol. To ensure that our results do not depend on individual parameter estimates

(which may be inaccurate), we based our analysis on sets of parameter estimates for which the coupled models behave consistently with the data; these sets define a confidence region (Figure 1D). Histograms of the relative auxin fluxes were generated using estimates from the confidence regions, which were robust to experimental and biological variation (Figure 1D), thus providing a means to elucidate the underlying mechanisms of nuclear auxin transport. We find consistent results from our analysis of the two responses, independently of the timescales involved.

### Accumulation of Fluorescent Auxin Analog in the Nucleus Is Not Driven by Diffusion Alone

It is generally considered that a small organic molecule such as auxin should diffuse freely between the cytosol and the nucleoplasm via the nuclear pores. In the context of auxin subcellular distribution, this would mean that the nucleoplasm and the cytosol could be conceptually treated as a single compartment. To test this assumption, we used the NBD-conjugated naphthalene-1-acetic acid (NAA) fluorescent auxin analog, NBD-NAA. NBD-NAA was shown to be active for auxin transport while remaining biologically inactive (Hayashi et al., 2014). The diester form of carboxyfluorescein (CF), 5(6)-carboxyfluorescein diacetate (CFDA), was included in the study as a control diffusion dye. Similar to auxins such as IAA and NAA, CFDA freely passes through the plasma membrane via diffusion, and once in the cell, the dye is hydrolyzed to acetic acid and negatively charged CF, a membrane-impermeable fluorescent probe (Oparka et al., 1994). In contrast to auxins, there are no known CFDA-specific transporter proteins. Both CF and NBD-NAA have carboxylic acid and similar molar masses (376.3 and 408.4 g·mol<sup>-1</sup>, respectively) that are higher than the molar mass of NAA (186.2 g·mol<sup>-1</sup>) yet well below what is considered the size exclusion barrier of nuclear pores (Görllich and Kutay, 1999).

Spatiotemporal changes in probe levels were monitored in living *Arabidopsis* protoplasts, a versatile analytical system to study cellular and subcellular processes in a uniform single cell population (Yoo et al., 2007). NBD-NAA could be detected in cells within 5 min of incubation (Figures 2A and 2C). The probe largely (maximum value at Pearson's R value, 0.79) co-localized with the ER-mCherry marker, as reported previously (Hayashi et al., 2014). This, together with a clearly more diffuse pattern, indicated availability of the fluorescent auxin analog in the cytosol as well. Surprisingly, however, the NBD-NAA signal in the nucleus appeared considerably weaker.

To compare changes in fluorescence intensity of NBD-NAA and CF in the nuclear and the extra-nuclear regions (cell excluding nucleus) over time, mCherry-tagged histone H2B (HTB4-mCherry) was transiently expressed as the nucleus marker (Figures 2B and 2C). Spatiotemporal tracking of cells at 5 min intervals showed that CF fluorescence intensity gradually increases in the cells and nuclei over a 30 min period (Figure 2B). The fluorescence intensity of NBD-NAA, however, remained relatively constant in both the nuclei and the whole cells (Figure 2C), suggesting that intracellular auxin levels were rapidly established and auxin-transport machinery constantly maintains a balance between cellular auxin influx and cellular auxin efflux.

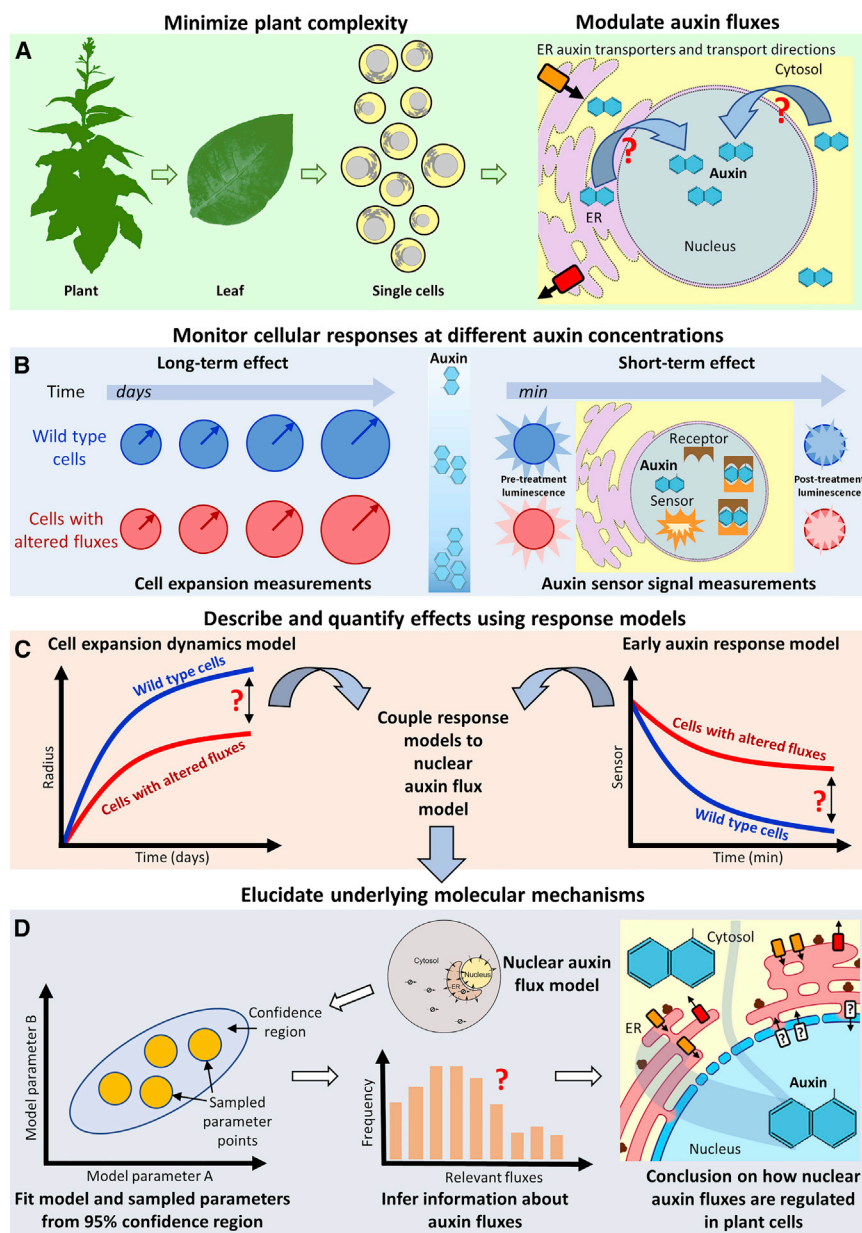


**Figure 1. Exploration Concept of Nuclear Auxin Uptake**

(A) Approach to efficiently modulate intracellular auxin fluxes in single plant cells.

(B) Experimental assays to assess auxin-mediated perturbations using cell expansion as a long-term response and the auxin sensor reporter system as a short-term response.

(C) Mathematical models are used to quantify the effect of auxin transport modulation on long-term and short-term responses. The models are then coupled to a model of perinuclear auxin fluxes.

(D) Coupled models are fitted to the expansion response data, yielding parameter estimates. Confidence regions of the parameter estimates (illustrated as parameters A and B) are sampled and subsequently used to generate distributions of the relevant auxin fluxes.

cence intensity for the nuclear and extra-nuclear regions should be similar and therefore lie along the diagonal of the quantile-quantile plot.

For NBD-NAA, the 5% quantiles (Figure 2D) fall along the diagonal line, implying that the least bright pixels of nuclear segments are similar in fluorescence intensity to the least bright pixels in the extra-nuclear segments (Figure S1B). However, the 95% quantiles for NBD-NAA (Figure 2D) lie below the line. This means that the brightest pixels in the nuclear segments are less bright than the brightest pixels in the extra-nuclear segments (Figure S1B). The corresponding quantile-quantile plot for CF (Figure S1D) shows that both the 5% and the 95% quantiles lie above the diagonal line, indicating that fluorescence intensities in the nuclear region are stronger than those in the extra-nuclear region. Thus, for both CF and NBD-NAA, the fluorescence intensity distribution in the nuclear region is different from the distribution in the extra-nuclear region.

To quantitate these ratios, we generated, for each cell, histograms of pixel intensities (distributions) of the whole cell and the nuclear and extra-nuclear regions (Figure S1A). Due to differences in uptake of the fluorescent probes by individual cells, there is significant inter-cellular variability in the median (Figure S1C). In addition, each distribution has a long tail (Figure S1B), so differences are most apparent when one considers the upper and lower quantiles. We therefore used quantile-quantile plots to compare the distribution of the ratios for both CF and NBD-NAA (Figures 2D–2E; Figures S1D and S1E) and normalized these quantiles by the medians to account for the inter-cellular variability. If one assumes that NBD-NAA and CF diffuse freely through the nuclear pores, then the quantiles of fluores-

Quantile-quantile plots were used to analyze time-dependent changes in NBD-NAA by comparing the distribution of NBD-NAA at 5 and 30 min (Figure 2E) for the same compartment. These show that the 5% and 95% quantiles lie along the diagonal line for both the nuclear and the extra-nuclear regions, confirming that NBD-NAA rapidly reaches equilibrium. In contrast, analogous quantile-quantile plots for CF (Figure S1E) show that all quantiles lie above the diagonal line for both regions, reflecting the gradual increase in CF intensity between the two time points.

Our results show that the movement of both CF and NBD-NAA between the nuclear and the extra-nuclear regions (and subsequently their nuclear accumulation over time) is not consistent with the simple conceptual model in which the nucleoplasm

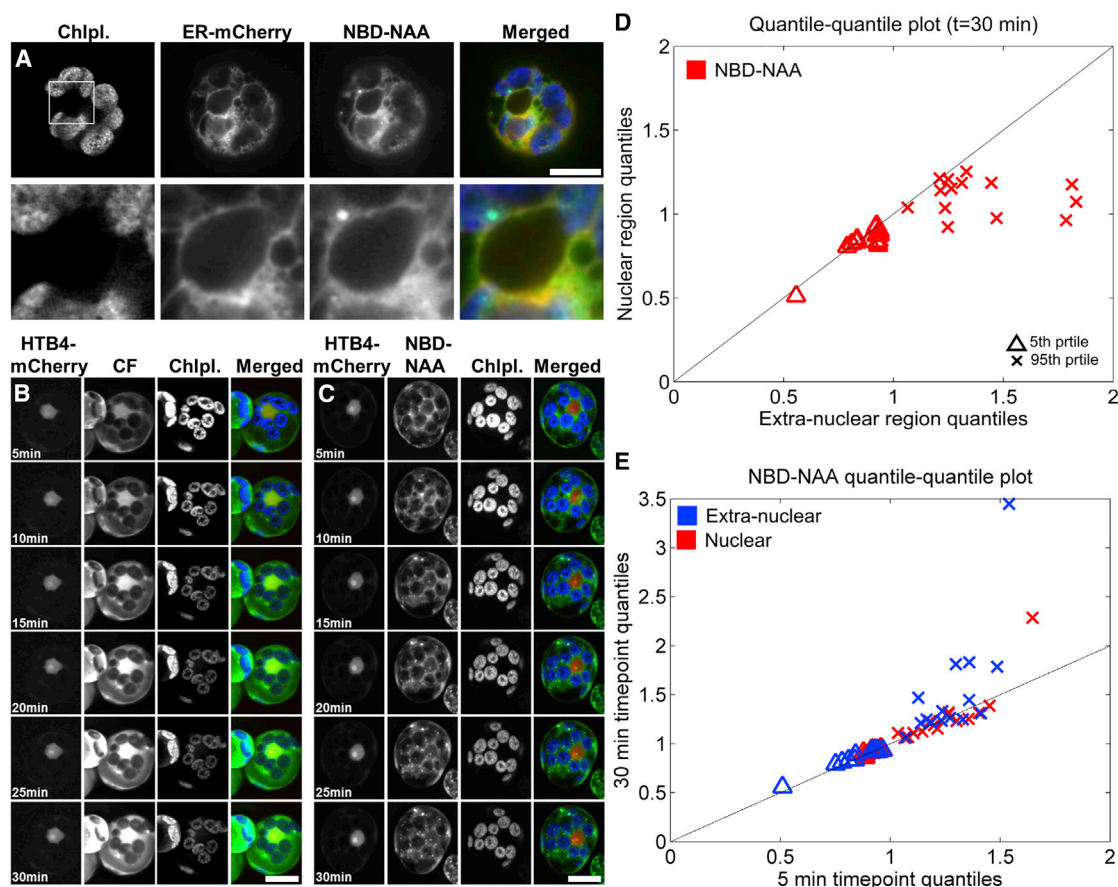


**Figure 2. Analysis of NBD-NAA and CF Dynamics in *Arabidopsis* Protoplast-Derived Cells**

(A) Co-localization of NBD-NAA (5 min treatment) and ER-mCherry marker (upper panel). A more diffuse NBD-NAA pattern and probe-specific accumulation sites (lower panel) around the nucleus were surrounded by chloroplasts (Chlpl). Scale bars correspond to 10  $\mu$ m.

(B and C) Time course study reveals distinct dynamics of CF and NBD-NAA in nuclear and extranuclear regions. 3D projections of representative cells incubated in medium supplemented with CFDA (B) or NBD-NAA (C). Image series were acquired at 5 min intervals, and the nucleus was identified using the HTB4-mCherry histone marker.

(D and E) Quantile-quantile plots of fluorescence in the nuclear and extra-nuclear regions using the 5th percentile (triangles) and 95th percentile (crosses) normalized against the median (50th percentile) for NBD-NAA-treated cells ( $n = 15$  per treatment) are as shown (D). Analogous quantile-quantile plots comparing the fluorescence distributions at 5 and 30 min for the nuclear and extra-nuclear regions separately (E).

See also [Figure S1](#).

and the cytosol can be treated as a single compartment, whereby small molecules can rapidly pass through the nuclear pores by passive diffusion. These results therefore indicate that the nuclear uptake of auxin is driven by processes other than diffusion.

### Modulation of Auxin Fluxes at the ER Affects Cell Division and Enhances Cell Expansion

We next developed genetic perturbation assays to understand the link between subcellular distribution of physiologically active auxin and downstream signaling responses. ER-localized auxin transporters PIN5 (Mravec et al., 2009) and PIN8 (Dal Bosco et al., 2012; Ding et al., 2012) were selected as potential molecular modulators of auxin fluxes between the cytosol and the ER. The chemically stable synthetic auxin NAA (Dunlap et al., 1986), which is, in contrast to NBD-NAA, a physiologically active com-

pound, was used to study cellular responses to auxin. Due to its hydrophobicity, NAA freely diffuses through the plasma membrane barrier (Delbarre et al., 1996).

We first confirmed co-localization of PIN5 and PIN8 with an ER marker in *Arabidopsis* and tobacco leaf protoplasts. Previous expression analysis of *PIN8* under native regulatory elements (Dal Bosco et al., 2012) showed no detection of this gene in *Arabidopsis* leaves. Therefore, the Cauliflower mosaic virus (CaMV) 35S promoter was selected to transiently overexpress PIN5-GFP and PIN8-GFP. PIN8-GFP was mainly co-localized with the ER-mCherry marker (Figure 3A), while transiently expressed PIN5-GFP was additionally observed in vesicle-like compartments (Figure S2A). After 48 hr of culture, PIN5-GFP was no longer observed in most cells, while transiently expressed PIN8-GFP or ER-YFP marker could be detected for more than a week (Figures S2B and S2C).

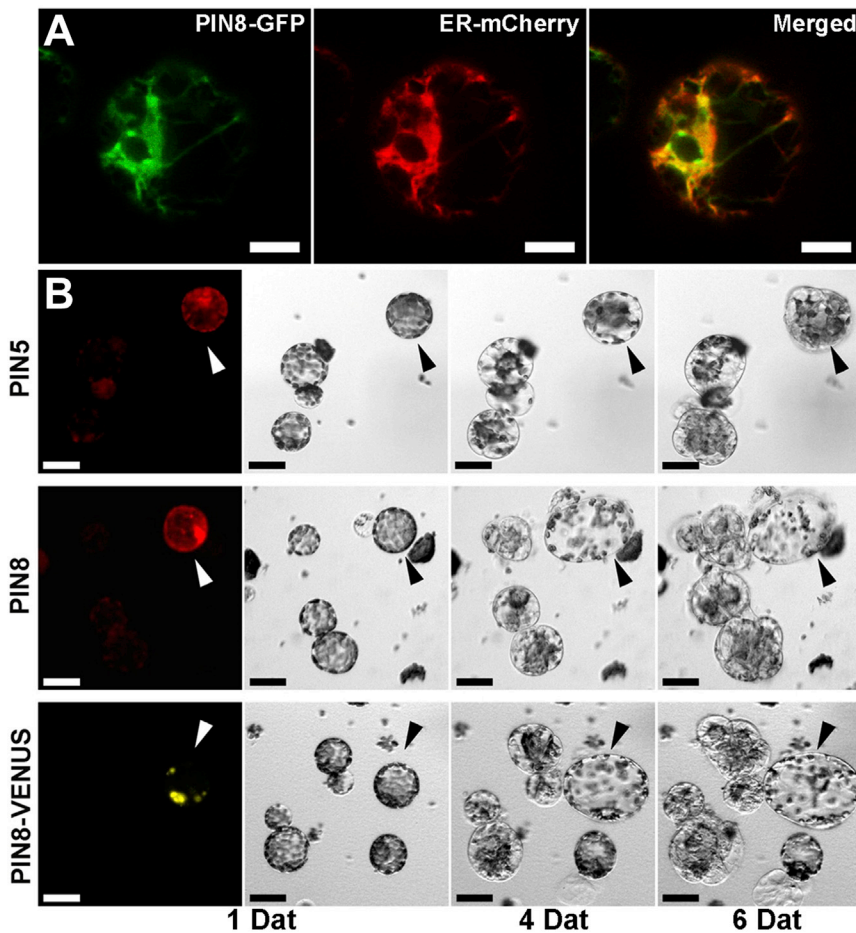
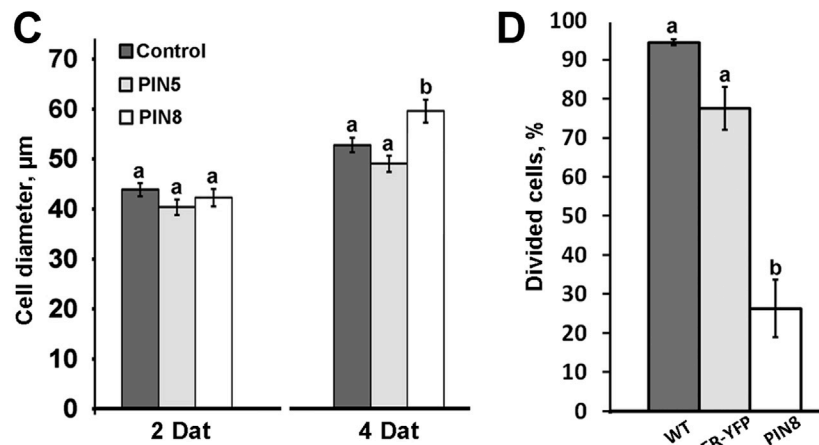


**Figure 3. Analysis of Modulation of Auxin Responses in Protoplast-Derived Cells**

(A) GFP-tagged PIN8 predominantly co-localizes with the ER marker mCherry-HDEL in *Arabidopsis* leaf protoplasts. Scale bars correspond to 5  $\mu\text{m}$ . (B) Upon overexpression, both VENUS-tagged and non-tagged PIN8, but not PIN5, result in enhanced cell expansion and arrest of cell divisions in transiently transformed tobacco leaf protoplasts. Arrowheads depict representative cells for each group tracked over 6 days after transformation (Dat). PIN8-expressing cells (arrowheads, middle and lower panels) did not divide at 6 Dat, whereas the non-transformed cells that survived the treatment and the PIN5-expressing cell (arrowheads, upper panel) underwent more than one cell division to this time point. Scale bars correspond to 20  $\mu\text{m}$ . (C) Analysis of morphometric changes in tobacco leaf protoplasts expressing the ER-YFP marker (Control), PIN5, or PIN8. Cells representing each group were manually tracked and analyzed. Error bars correspond to SE ( $n = 26$ ). Statistically significant different groups at each time point are indicated with lowercase letters (one-way ANOVA,  $p < 0.001$ ). (D) Comparison of division frequency between non-transformed tobacco leaf protoplasts (WT) and protoplasts expressing ER-YFP or PIN8. Manual tracking and analysis of cell divisions (WT,  $n = 106$ ; ER-YFP,  $n = 102$ ; PIN8,  $n = 88$ ) were performed in 3 independent experiments. Statistically significant different groups are indicated with lowercase letters (one-way ANOVA,  $p < 0.0002$ ). See also [Figures S2 and S3](#).



The expansion and division of single cells are commonly exploited as physiological markers of auxin effects (Campanoni and Nick, 2005). Therefore, these parameters were assessed in immobilized tobacco leaf protoplasts to quantify consequences of perturbed intracellular auxin fluxes at the ER.

To ensure that functional properties of transiently overexpressed PINs in protoplasts were not affected by translational fusion with the fluorescent tags, tagged and non-tagged ver-

sions of tested PINs were compared by manual tracking of immobilized transformed cells at 24 hr intervals. In a case of using non-tagged PINs, an additional fluorescence reporter gene encoding the cytosolic mCherry protein was cloned in the expression plasmids. This strategy enabled identification of cells of interest (expressing non-tagged PINs) by detecting the mCherry fluorescence signal (Figure 3B). After 2 days of culture in the presence of 0.5  $\mu\text{M}$  NAA, no statistically significant difference in cell sizes could be found among samples transformed with PIN5, PIN8, or ER-marker control (Figure 3C). In contrast, 3- to 4-day-old cells overexpressing non-tagged PIN8

were significantly larger than the control cells or PIN5-overexpressing cells (Figure 3C). Cells expressing non-tagged or tagged PIN8 (Figure 3B) showed a similar behavior in cultures, thus suggesting that function of PIN8 in protoplasts is not affected upon protein tagging with the yellow fluorescence marker VENUS. Furthermore, cell divisions in PIN8-overexpressing cells were strongly suppressed (Figures 3B and 3D; Figure S2B). This, together with the elevated cell expansion

behavior, resembles the auxin-starvation phenotype observed in tobacco suspension cells under auxin-deprived conditions (Winicur et al., 1998).

Overall, these results showed that (1) an immobilized protoplast-derived cell model represents a potent experimental platform to quantitatively analyze cell expansion dynamics and (2) perturbation of auxin fluxes at the ER obtained by overexpression of PIN8 (but not of PIN5) affects cell expansion. We therefore chose PIN8 gain-of-function mutant (PIN8OX) as a tool for modulating intracellular auxin fluxes in cell expansion studies using immobilized protoplasts.

### Cell Expansion Dynamics Model Indicates a Mechanism Regulating Nuclear Auxin Levels

Current methods for the immobilization of single plant cells, which cannot grow by adhering to a surface, are not optimized for microscopic multi-time point observations, especially for medium- to large-scale experimental setups. To overcome this, we developed an approach, named protoplast monolayer embedding (PME), for efficient and robust immobilization of protoplast-derived cells directly in multi-well plates (Figure S3A). To quantitatively study cell expansion dynamics from microscopic 4D image sequences, we next developed AutoOvuscule, a computational tool for automated segmentation, tracking, and measurement of cell morphology over time and discriminating living and dead cells (Figure S3B). Immobilized protoplasts can be observed over continuous intervals (days to weeks) under diverse culture conditions (Figures S3C–S3J).

In earlier studies, it was shown that auxin stimulates swelling of freshly prepared protoplasts (Steffens and Lüthen, 2000; Steffens et al., 2001). There, volumetric changes were monitored in cells lacking the cell wall. In this study, we monitored expansion of the cells after recovery of the cell wall, because genetic and pharmacologically induced modulations of the extracellular matrix have demonstrated crosstalk between auxin and cell wall function (Feraru et al., 2011; Steinwand et al., 2014). The cell wall of tobacco protoplasts is recovered within 24 hr, even in auxin-free culture conditions (Figure S4A). Immobilized tobacco leaf protoplasts from wild-type (WT) or PIN8OX (Dal Bosco et al., 2012) were used to quantitatively assess cell expansion in response to a range of auxin concentrations (Figures S4B and S4C). Acquired image time series of cultured protoplasts were processed using AutoOvuscule to automatically track individual cells, identify their status (dead or alive), and measure diameters at each time step. Divided and non-divided cells cannot be discriminated using the tool, because daughter cells occupy the same space as a parent cell after the initial cell division (Figure S5A). Therefore, 72 hr was selected as a terminal time point. According to expert-guided image inspection, initial cell divisions could be clearly identified at this time point in WT or PIN8OX PME cultures incubated with 0.5–25 or 5–50  $\mu\text{M}$  NAA, respectively. Cells that had died during the 72 hr observation period were excluded from the analysis. Averaged values of cell diameters were plotted against time for the different experimental conditions (Figure 4A) and visualized as histograms of cell diameters for individual conditions and time points (Figure S5B).

We observed that WT cells cultured in auxin-free conditions initially expanded at a constant rate before decelerating notice-

ably by 48 hr (Figure 4A). In cells treated with sub- and micromolar concentrations of NAA, the deceleration of expansion occurred even earlier (Figure 4A). In contrast, PIN8OX cells treated with concentrations of NAA up to 5  $\mu\text{M}$  expanded at an approximately constant rate, so no significant deceleration could be observed (Figure 4A). Only for cells cultured in the presence of very high concentrations of NAA (10–50  $\mu\text{M}$ ) was a deceleration phase observed within 72 hr (Figure 4A). The highest auxin concentration tested (50  $\mu\text{M}$  NAA) was toxic for WT cells, but not PIN8OX cells (Figures S4B and S4C). This decreased sensitivity of PIN8OX cells to toxic NAA concentration, in concert with auxin-insensitive cell expansion rates at auxin concentrations below 5  $\mu\text{M}$  (Figure 4A; Figures S4B and S4C), consistently indicated that PIN8-mediated changes in the ER auxin pool resulted in significantly decreased responsiveness of cells to exogenous auxin.

We next sought a simple model enabling quantification of the cell expansion dynamics. Because cell diameter measurements at each time point and experimental condition were observed to be normally distributed (Figure S5B), we reasoned that a good description could be obtained by basing the model on the averaged cell expansion data (Figure 4A), rather than developing a more complex model describing the expansion of individual cells.

We assumed that changes in average cell volume are best captured by logistic growth. This model (Figure 4B) contains two parameters: the initial expansion rate ( $\alpha$ ), which defines over what timescale the cell might reach its maximal volume, and the maximal cell volume ( $V_{\text{max}}$ ). At larger timescales, cell alphas will decrease until steady-state volume  $V_{\text{max}}$  is attained (Figure 4C). To fit the model to the data and avoid overfitting, we adopted the simplest assumption, namely, that auxin regulates only one of the two model parameters. Because the relationship between the concentration of exogenous auxin and the value of these parameters was unknown, we fitted each experimental condition separately. We found that auxin regulation of the  $V_{\text{max}}$  reproduced the experimental data significantly better (Figure 4A) than regulation of the cell  $\alpha$  (Figure S5C). Best-fit parameter estimates are illustrated in Table S1.

In both PIN8OX and WT cells,  $V_{\text{max}}$  decreased with increasing exogenous NAA concentration, whereas  $V_{\text{max}}$  was always larger in PIN8OX cells than in WT ones (Figure 4D). WT cells exhibited a strong response of  $V_{\text{max}}$  to NAA concentrations below 2.5  $\mu\text{M}$  but a weak response above 2.5  $\mu\text{M}$ . In contrast, the response range of PIN8OX cells was extended. At 10  $\mu\text{M}$  NAA, the  $V_{\text{max}}$  of PIN8OX cells was comparable to that of untreated WT cells, while at 50  $\mu\text{M}$  NAA, the  $V_{\text{max}}$  was comparable to that of WT cells treated with 2.5  $\mu\text{M}$ . This illustrates that modulation of the ER NAA pool results in a substantially altered response of  $V_{\text{max}}$  to exogenous NAA.

Our data and the cell expansion model indicate links among exogenous auxin, modulation of the auxin flux at the ER, and cell expansion dynamics. While exogenous auxin showed a pronounced concentration-dependent inhibition of cell expansion, cell expansion per se is a highly complex process in which numerous direct and indirect auxin-triggered responses and auxin-independent events are coordinated over a long period. We therefore further explored how dynamic changes of cytosolic and ER-auxin pools influence nuclear auxin signaling.

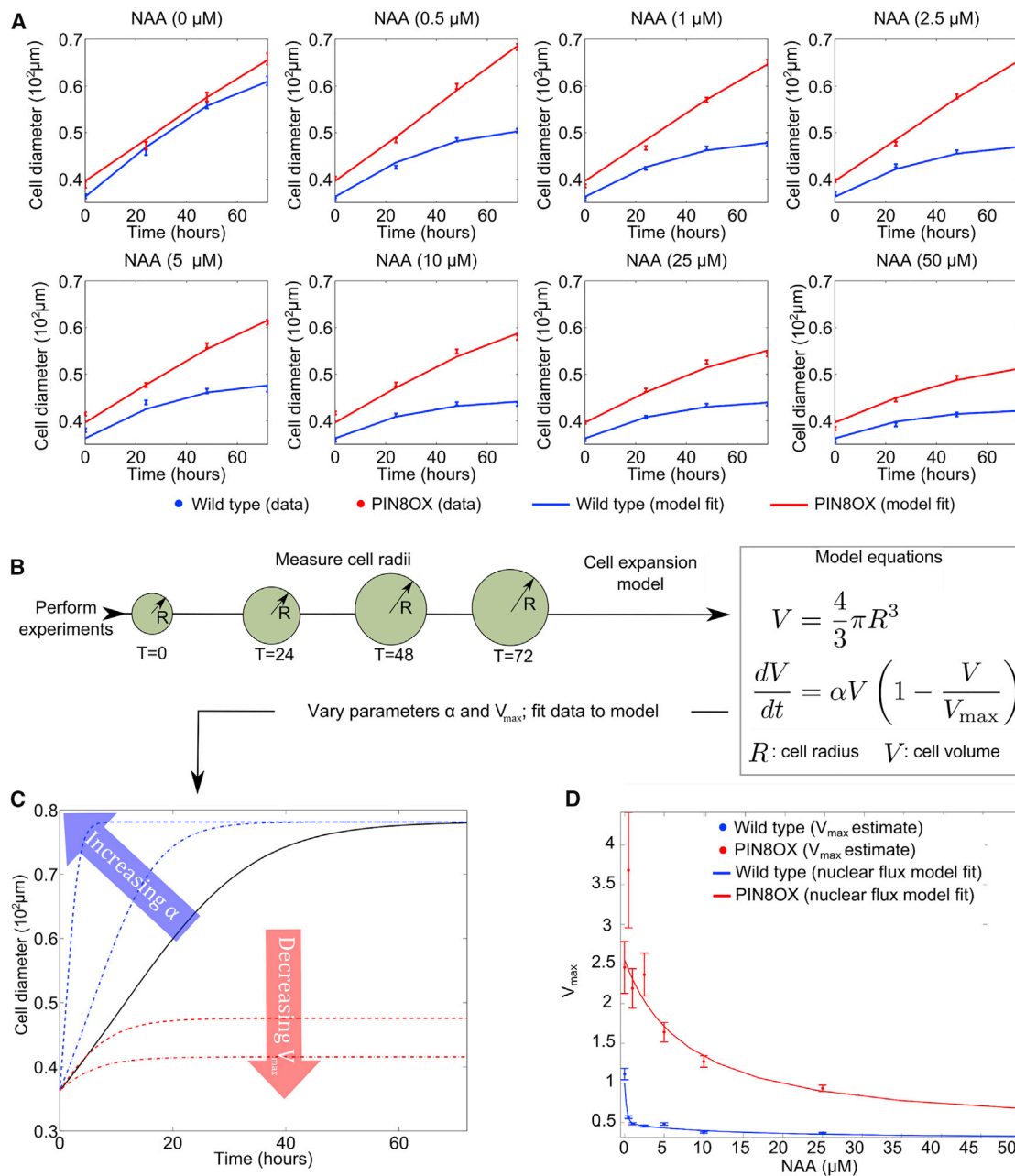


**Figure 4. Modeling and Analysis of Cell Expansion Dynamics**

(A) Changes in cell diameter over time for WT (in blue) and PIN8OX (in red) cells treated with different concentrations of NAA. Dots correspond to experimental data, and solid lines correspond to cell expansion model fits. Error bars correspond to SE (based on 5,115 PIN8OX cells and 5,471 WT cells).

(B) Pipeline relating cell radii measurements ( $R$ ) to the cell expansion model. Radii are used to calculate a cell volume ( $V$ ). The model assumes that changes in volume can be captured by logistic growth.

(C) Model parameter alpha ( $\alpha$ ) controls the time it takes for the cell to reach its maximal volume. The maximal volume is controlled by the parameter  $V_{\max}$ .

(D) Mean and SD of the confidence region for estimates to  $V_{\max}$  (normalized so that  $V_{\max}$  is 1 for untreated WT cells) plotted against the concentration of exogenous NAA for both WT and PIN8OX cells.

See also [Figures S3–S5](#) and [Table S1](#).

### Regulation of Auxin-Induced Genes *IAA1* and *IAA5* Is Affected in PIN8OX Cells

To test how differences in the cell expansion dynamics are correlated with altered nuclear auxin signaling, we analyzed the

expression of *IAA1* and *IAA5*, which are among the fastest auxin-induced genes (Abel et al., 1995), in protoplast-derived cells. Cells from *Arabidopsis* WT or PIN8OX were incubated for 1 hr at various concentrations of NAA. The qRT-PCR analysis

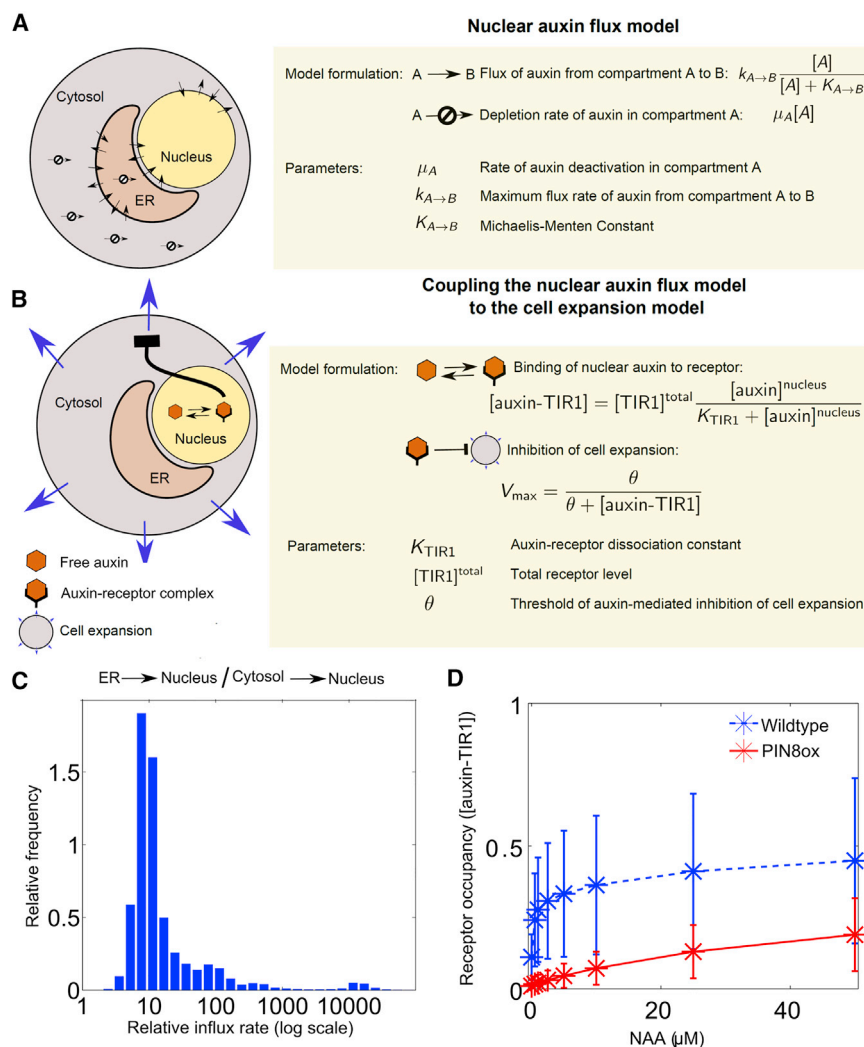


**Figure 5. Modeling of Nuclear Auxin Fluxes**

(A) Left: graphical depiction of the nuclear auxin flux model. The model describes auxin fluxes among the nucleus, the cytosol and the ER, together with depletion of auxin in the cytosol and ER. Right: flux of auxin from one compartment (compartment A) to another (compartment B) depends on the concentration of auxin in compartment A. This is modeled using a Michaelis-Menten function. The depletion rate of auxin in compartment A is assumed to be proportional to its concentration. Concentrations are denoted by square brackets.

(B) Left: graphical depiction of the coupling between the nuclear auxin flux model and the cell expansion model (Figure 4), wherein cell expansion is inhibited by nuclear auxin signaling. Right: level of nuclear auxin signaling represented by auxin-receptor occupancy (given by a Michaelis-Menten function); the maximal cell volume ( $V_{\text{max}}$ ) is assumed to be a decreasing function of the auxin-receptor occupancy.

(C) Histogram of relative nuclear auxin influx rates based on fits between the nuclear auxin flux model (A and B) and estimates of  $V_{\text{max}}$  (Figure 4D).

(D) Mean and SD of the predicted levels of nuclear auxin-receptor occupancy for PIN8OX and WT cells.

See also Table S2.

showed that expression levels of both *IAA1* and *IAA5* in PIN8OX cells were significantly lower than in the WT cells at all concentrations tested (Figures S6A and S6C). This confirmed that PIN8 directly interfered with the auxin cellular responses. Time-resolved analysis of *IAA1* and *IAA5* at 1  $\mu\text{M}$  NAA showed that prolonged incubations with auxin only partially rescued the expression levels of either gene (Figures S6B and S6D). These results are consistent with reduced expression of auxin responsive genes in PIN8OX previously observed *in planta* (Dal Bosco et al., 2012). Changes in expression levels of auxin-induced genes in WT and PIN8OX cells indicate that the altered response of  $V_{\text{max}}$  to exogenous NAA in the cell expansion model and the nuclear auxin levels are interconnected.

### Mathematical Modeling Predicts the ER as the Main Conduit for Nuclear Auxin Flux

We next sought to understand how alteration of the auxin fluxes at the ER modulated nuclear auxin signaling by developing a mathematical model of nuclear auxin fluxes. Because no methods directly demonstrate transport directionality of intracel-

lular auxin transporters, such as PIN8, we assumed that PIN8 transports auxin from the ER into the cytosol due to the following rationale. Radioactive auxin transport assays performed on whole cells, which were independently performed by different research groups (Ding et al., 2012; Ganguly et al., 2010), consistently showed decreased accumulation of the hormone in PIN8OX cells in comparison to the control cells. Therefore, these data exclude accumulation of auxin due to intracellular compartmentalization (which otherwise would lead to the increased radioactivity within the cells) and corroborate the assumption that PIN8 transports auxin from the ER into the cytosol, from which it is exported out of the cells by the efflux machinery.

Our data on subcellular distribution of the fluorescent auxin analog NBD-NAA (Figure 2; Figure S1) suggested that auxin uptake into the nucleus does not occur via simple diffusion. The nuclear auxin flux model (Figure 5A) assumes that auxin is exchanged among the cytosol, the nucleus, and the ER. Thus, there are two fluxes into the nucleus: one via the ER and one via the cytosol. The relative strength of these different fluxes is determined by the model parameters, which are estimated by fitting the model to experimentally derived  $V_{\text{max}}$  values (Figure 4D). To describe the flux of auxin between compartments A and B, we used saturating transport functions (Figure 5A). This approach captures both linear and non-linear transport behavior by adjusting the associated constant  $K_{A \rightarrow B}$ . Additional model parameters (for details, see Supplemental Experimental

Procedures) reflect the maximal rate of auxin flux ( $k_{A \rightarrow B}$ ) and rates of auxin depletion ( $\mu_A$ ). To capture the difference between PIN8OX cells and WT, we assume that PIN8OX cells have an increased auxin flux from the ER to the cytosol when compared to WT ones.

Based on the observed functional dependence of  $V_{\max}$  on exogenous NAA, we took  $V_{\max}$  to be a decreasing function of the level of nuclear auxin (Figure 5B, right panel). As noted earlier, steady-state intracellular auxin levels appear to be established within minutes of treatment (Figures 2C and 2E) and hence operate on a much faster timescale than that of growth (days). We therefore assumed that the nuclear auxin flux model is at steady-state and fitted our nuclear auxin flux model to the estimates of  $V_{\max}$  (Figure 4D, solid lines). To understand how differences between WT and PIN8OX  $V_{\max}$  curves are reflected in the parameters of the nuclear auxin flux model, we first performed a global parameter scan to estimate the 95% confidence region of the parameter estimates (Table S2). We then calculated the ER-to-nucleus or cytosol-to-nucleus auxin flux ratio (for details, see Supplemental Experimental Procedures) for each parameter set inside the confidence region (Figures 1D and 5C).

In every case, flux from the ER to the nucleus was predicted to be significantly larger than flux of auxin from the cytosol, with a median 10-fold difference between the two (Figure 5C). In other words, the model predicts that of the two fluxes into the nucleus, the ER-to-nucleus one dominates over the cytosol-to-nucleus flux. The corresponding receptor occupancies (Figure 5B, model formulation) were also calculated for each parameter set taken from the confidence region: occupancy in PIN8OX cells is maintained at a level (regardless of the exogenous auxin concentration) that is 2–4 times lower than that in WT (Figure 5D). Similar fold changes in gene expression between WT and PIN8OX cells were determined in our qRT-PCR experiments (Figures S6A–S6D). Hence, our model indicates that the observed differences between PIN8OX and WT cells can be largely attributed to alterations in nuclear auxin transport.

To further explore and to validate our model predictions, we exploited a recently developed quantitative genetically encoded auxin sensor (Wend, et al., 2013).

### Early Nuclear Auxin Response Model Suggests ER-to-Nucleus Transport Mechanism in Regulation of Nuclear Auxin Levels

The functional principle of the sensor, similarly to the DII-VENUS reporter (Brunoud et al., 2012), relies on the auxin-mediated formation of the TIR1/AFB-Aux/IAA-like complex such that the sensor activity directly relates to the nuclear auxin abundance. In addition to an auxin responsive module (firefly luciferase translationally fused with the conserved degron motive of Aux/IAAs), the sensor comprises an auxin-insensitive module (Renilla luciferase), which serves normalization purposes. The luminescent nature of the modules provides higher sensitivity than fluorescent probes. Upon expression of the sensor in plant cells, auxin-mediated degradation of the responsive module is monitored as a relative decrease of firefly luciferase luminescence to Renilla luciferase luminescence. Therefore, the degradation kinetics of the sensor reflects alterations in nuclear auxin levels as close to real time as possible.

We first generated time-resolved auxin dose-response data of the sensor for WT and PIN8OX cells (Figure 6A). *Arabidopsis* leaf protoplast cells expressing the sensor were incubated with different concentrations of NAA (0, 0.1, 0.5, 1.0, and 2.5  $\mu\text{M}$ ). Sensor levels were measured immediately after treatment and then at regular intervals up to 1 hr. In WT cells, sensor levels began to reduce almost immediately after NAA application: at the highest NAA concentration, sensor levels dropped by as much as 40% in the first few minutes. However, in PIN8OX cells, the sensor degradation kinetics was noticeably slower (Figure 6A).

We next developed an early nuclear auxin response model using the sensor data to ascertain how differences in the sensor degradation kinetics might correspond to altered nuclear auxin levels (Figure 6B). The model takes into account interactions among auxin, its receptors (TIR1/AFBs), and the sensor (for details, see Supplemental Experimental Procedures). As with  $V_{\max}$  in the cell expansion model (Figure 4), the relationship between the auxin treatment level and the concentration of nuclear auxin is unknown. Therefore, parameters associated with these interactions, together with the level of nuclear auxin, were estimated by fitting the model to the sensor data (Figure 6B, parameters panel). Sensor responses were measured on timescales at which *de novo* synthesis of auxin receptors can be assumed to be negligible.

As before, we performed a global parameter scan to approximate the 95% confidence region of the parameter estimates for the early nuclear auxin response model (Table S3). In Figure 6C, we plotted the receptor occupancy for both WT and PIN8OX cells against the concentration of exogenous NAA. In broad agreement with our quantitative analysis of the cell expansion data (Figure 4), receptor occupancy was reduced by 6-fold in PIN8OX cells when compared to WT (Figure 6C).

We next checked predictions of the model for the natural auxin IAA (Table S4). Overall, both the sensor dynamics (Figure S6E) and the resulting receptor occupancy (Figure S6F) were similar to the ones found for NAA (Figures 6A and 6C). We observed that the receptor occupancy measured for IAA saturates at a lower concentration of exogenous IAA than for NAA. This is consistent with the reported lower binding affinity of TIR1 to NAA (Dharmasiri et al., 2005; Kepinski and Leyser, 2005).

Finally, we tested our prediction that auxin enters the nucleus predominantly via the ER. We parameterized the nuclear auxin flux model (Figure 5A; Table S2) by fitting it to the receptor occupancy estimates from the sensor data. The resulting dose-response curves and the corresponding fits for NAA or IAA are shown in Figure 6C and Figure S6F, respectively. Then, as with the cell expansion model (Figure 5C), we calculated the ER-to-nucleus or cytosol-to-nucleus auxin flux ratio for each parameter set inside the 95% confidence region. This revealed strikingly similar histograms for NAA (Figure 6D) and IAA (Figure S6G) flux ratios. According to the median of the flux ratio distribution, the ER-to-nucleus NAA flux is 46-fold stronger than the cytosol-to-nucleus fluxes. This indicates an even larger flux ratio than was predicted by our analysis of the cell expansion dynamics. For IAA, the median flux ratio predicts an 84-fold stronger ER-to-nucleus flux compared to the cytosol-to-nucleus fluxes. Altogether, the early nuclear auxin response model confirms two key predictions made using the cell expansion dynamics data and the nuclear auxin flux models (Figures 4 and 5), namely, that

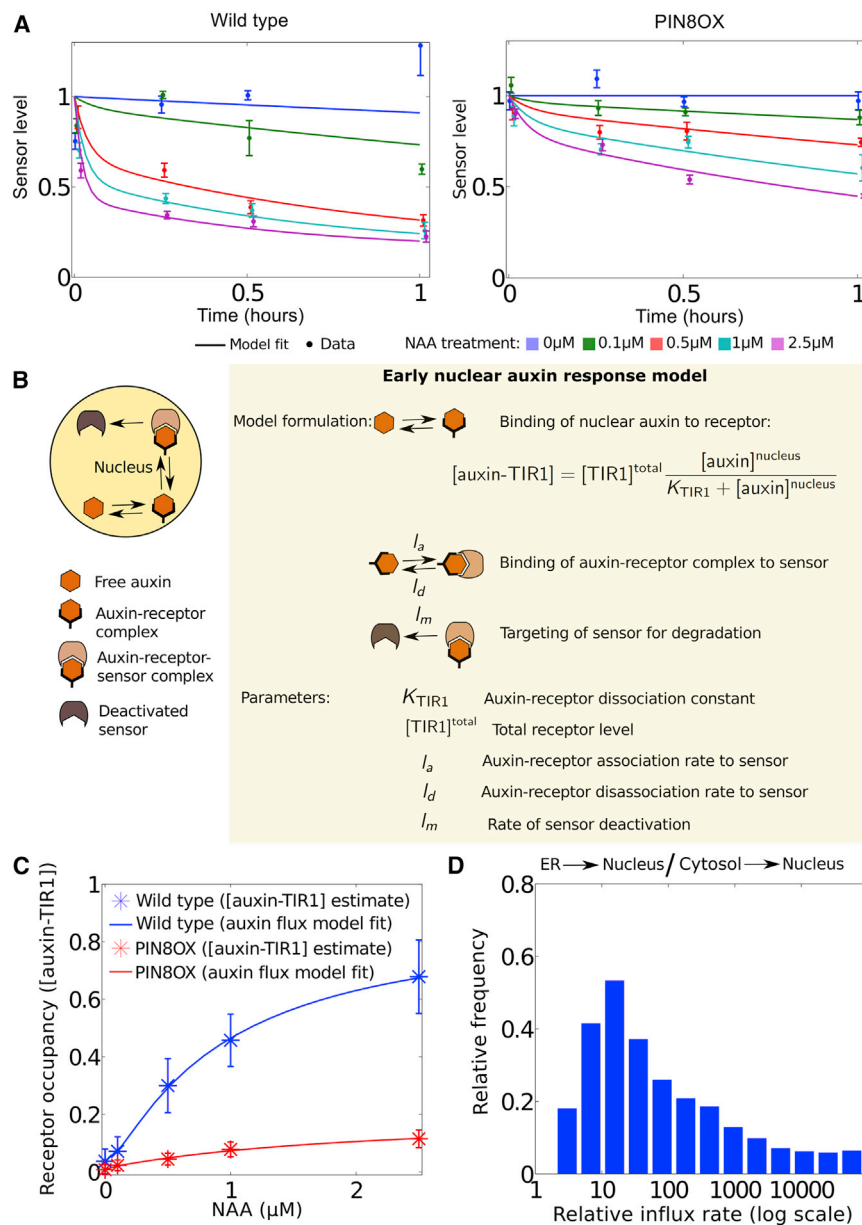


**Figure 6. Modeling of Early Nuclear Auxin Response and Validation of the Nuclear Auxin Flux Model Using Ratiometric Auxin Sensor**

(A) Changes in sensor levels over time for either WT or PIN8OX cells treated with various concentrations of NAA. Dots correspond to experimental data, and solid lines correspond to early nuclear auxin response model fits. Error bars correspond to SE (n = 5).

(B) Left: graphical depiction of the early nuclear auxin response model. Right: nuclear auxin binds to its receptor, and then this forms a complex with the sensor. The sensor is then targeted for degradation. Concentrations are denoted by square brackets. Model parameters are as given.

(C) Mean (stars) and SD (error bars) of the receptor occupancy (calculated using parameters taken from the 95% confidence region) plotted against the concentration of exogenous NAA for both WT and PIN8OX cells. Estimates are based on fits between the early nuclear auxin response model and the data (A). The nuclear auxin flux model (Figure 5A) is then fitted directly to the receptor occupancy data (solid lines).

(D) Histogram of relative NAA fluxes, based on fits between the nuclear auxin flux model and the receptor occupancy curves (B and C). See also Figure S6 and Tables S2–S4.

plained by a rapid degradation of PIN5 within 48 hr. However, short-term effects should still be present and therefore detectable with the auxin sensor. PIN5 likely transports auxin from the cytosol to the ER and therefore in the opposite direction of PIN8. This has been demonstrated with radioactive auxin transport assays (Mravec et al., 2009), which show decreased efflux (and hence increased retention) of auxin in PIN5OX cells in comparison to control. A natural question arises: What is the effect of overexpressing PIN5 on nuclear auxin fluxes?

To explore this further, we used the parameter sets sampled from the 95% confidence regions already obtained by fitting the WT and PIN8OX sensor data (Tables S3 and S4) to the early nuclear auxin response model (Figure 6C; Figure S6F) and assumed (consistent with the work of Mravec et al., 2009) that overexpression of PIN5 results in an increase of cytosol-to-ER auxin flux. As a consequence, our model predicts a decrease in cytosol levels of auxin in favor of ER ones. This results in one of two consequences for nuclear auxin uptake. In scenario 1, the increase in ER-to-nucleus flux is greater than the decrease in cytosol-to-nucleus flux, so the net effect is an increase of nuclear auxin levels (and hence increased receptor occupancy). In scenario 2, the opposite occurs, whereby the decrease in cytosol-to-nucleus flux is greater than the increase in ER-to-nucleus flux, resulting in a decrease in nuclear auxin levels (and hence decreased receptor

(1) the difference in nuclear auxin signaling between PIN8OX and WT cells is established almost immediately after treatment and (2) receptor occupancy in PIN8OX cells is maintained at a low level as exogenous auxin levels are increased. Although the predicted ER-to-nucleus flux rates derived using the sensor are higher than those predicted from the cell expansion dynamics model, both models suggest a dominant role of the ER and the ER-to-nucleus flux in regulating nuclear levels of the phytohormone auxin.

### Early Nuclear Auxin Response Model Explains Opposing PIN5 Overexpression Effects

The cell expansion data did not reveal any significant effect of PIN5 overexpression (Figures 3B and 3C), which could be ex-

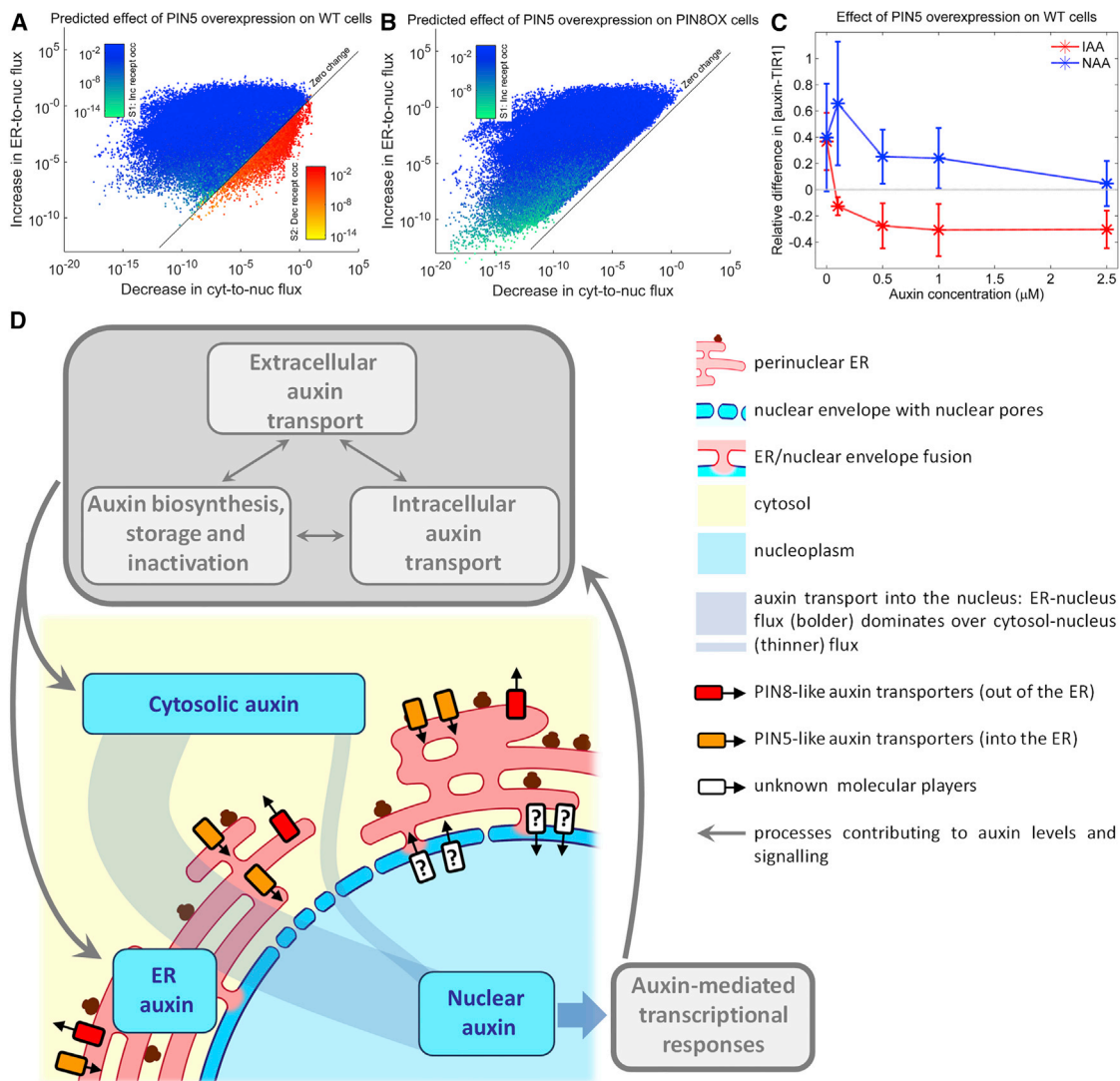


**Figure 7. The ER Acts as a Gateway for Controlling Nuclear Auxin Levels**

(A and B) Data-driven modeling explains opposing PIN5 responses and predicts that auxin predominantly enters the nucleus via the ER. Scatterplot of predicted loss in cytosol-to-nucleus flux against gain in ER-to-nucleus flux following PIN5 overexpression for WT (A) and PIN8OX cells (B) treated with  $2.5 \mu\text{M}$  of IAA. Points are color-coded to reflect change in nuclear receptor occupancy. Axis given in logscale. S1, scenario 1; S2, scenario 2.

(C) Experimentally measured differences in receptor occupancy between WT and WT+PIN5 cells treated with IAA and NAA, relative to WT levels (see Figures S7A and S7C for the corresponding absolute levels).

(D) Fluxes between the ER and the cytosol are mediated by specific efflux and influx carriers such as PIN5, PIN8, and PILS proteins. Hitherto unidentified molecular players likely mediate fluxes between the ER and the nucleus. Fluxes between the cytosol and the nucleus are still predicted to occur, albeit at a significantly slower rate. Thus, a key step in regulating nuclear auxin levels occurs directly at the ER.

See also Figures S7 and S8 and Table S2.

occupancy). To visualize this, we plotted for each parameter set the predicted gain in ER-to-nucleus flux against the loss in cytosol-to-nucleus flux (Figures 7A and 7B), where blue points correspond to scenario 1 (increase in receptor occupancy) and red points correspond to scenario 2 (decrease in receptor occupancy). Points that lie along the diagonal correspond to the cases in which increase in ER-to-nucleus flux is balanced by decrease in cytosol-to-nucleus flux, leading to no net change in the receptor occupancy and nuclear auxin levels. In WT cells overexpressing PIN5 (WT+PIN5), both scenarios are predicted to be possible, de-

pending on a given parameter set (Figure 7A). In contrast, for PIN8OX cells overexpressing PIN5 (PIN8OX+PIN5) only scenario 1 is predicted to occur, although the magnitude of the increase in nuclear auxin could be rather low and below the level of detection (Figure 7B). Similar predictions were made independent of the concentration or type of auxin used.

We next sought to test these predictions by co-expressing the auxin sensor and PIN5 in WT or PIN8OX cells. For this, we used the early nuclear auxin response model (Figure 6) to obtain fits (within 95% confidence regions) to time-resolved IAA and NAA

dose-response data (Figures S7A–S7D) to gain information about corresponding receptor occupancies (Figures S7E and S7F). To more clearly visualize the effect of PIN5 overexpression, we plotted (for both NAA and IAA) the difference in receptor occupancies between WT and WT+PIN5 cells (Figure 7C) and the difference in receptor occupancies between PIN8OX and PIN8OX+PIN5 cells (Figure S7G). Untreated WT+PIN5 cells showed increased receptor occupancy when compared to WT (Figure 7C). This is consistent with the assumption that PIN5 increases cytosol-to-ER flux, leading to an increase in ER-to-nucleus flux and hence an increase in the nuclear steady-state concentration of auxin. However, as the concentration of exogenous auxin is increased, there is clear divergence in the response: overexpression of PIN5 leads to an increase in NAA receptor occupancy, whereas for the IAA receptor, occupancy is reduced when compared to WT (Figure 7C). In contrast, overexpression of PIN5 did not greatly affect receptor occupancy in PIN8OX cells for either IAA or NAA (Figure S7G).

The response of WT+PIN5 cells to NAA (Figure 7C) corresponds to scenario 1 in Figure 7A, whereas the IAA response corresponds to scenario 2. To understand what underpins the difference between these two scenarios in the model, we performed a further inspection of the corresponding parameter sets (for details, see Supplemental Experimental Procedures and Figure S8). This revealed that for parameters corresponding to scenario 2 (which we associate with IAA) the ER-to-nucleus flux rate reaches saturation. As a consequence, overexpression of PIN5 does not lead to a significant increase in the ER-to-nucleus flux, rather to the decrease in cytosol-to-nucleus flux, which results in decreased nuclear auxin levels and hence receptor occupancy. For parameters corresponding to scenario 1 (which we associate with NAA), ER-to-nucleus flux is not saturated, so a decrease in cytosol-to-nucleus flux is compensated by the increase in ER-to-nucleus flux. Thus, the model offers a consistent explanation for opposing effects of PIN5 overexpression in WT cells upon treatment with different auxins (Figure 7C). Overall, our results propose that (1) there are two routes for auxin to enter the nucleus, one via the ER and one via the cytosol; (2) the ER-to-nucleus flux dominates over the cytosol-to-nucleus one; and (3) the ER-to-nucleus flux can be saturated at high concentrations of auxin. In effect, the ER can act as conduit to the nucleus, unless the processes controlling ER-to-nucleus flux become saturated by auxin (for example, by overexpressing PIN5), in which case, it can act as a sink.

## DISCUSSION

In this work, we focused on unexplored aspects in auxin biology: whether and how auxin transport into the nucleus is regulated. To our knowledge, so far these questions have not arisen, likely due to the general assumption—without experimental evidence—that a small molecule such as auxin can freely diffuse from the cytosol into the nucleoplasm through the nuclear pores.

Taking advantage of auxin transport probes (Hayashi et al., 2014) we revealed unexpected intracellular dynamics of auxin that cannot be explained by simple diffusion alone. This parallels findings on the even smaller signaling molecule  $\text{Ca}^{2+}$ , which showed distinct  $\text{Ca}^{2+}$ -mediated responses in the nucleoplasm

and the cytosol (Charpentier and Oldroyd, 2013). Furthermore, it has emerged that in addition to size exclusion, the biopolymer matrix within the nuclear pores might function as a selective diffusion barrier for particular molecules by employing filtering mechanisms based on hydrophobic-electrostatic interactions (Lieleg and Ribbeck, 2011). This could affect auxin diffusion through the nuclear pores. Therefore, based on the observed distribution of the NBD-NAA between the nucleus and the extra-nuclear regions, we assumed the existence of an alternative mechanism to regulate nuclear auxin levels.

One of the first attempts to model cellular auxin dynamics in the context of auxin fluxes and ionic transport among apoplast, cytosol, and vacuole was carried out by Steinacher et al. (2012). The proposed framework has led to a number of predictions that remain to be experimentally tested. Here we developed a joint theoretical-experimental approach to circumvent the lack of tools for directly estimating how and what changes in subcellular auxin pools trigger what downstream responses. We exploited the relative simplicity of single plant cell systems and demonstrated that by overexpressing ER-localized auxin efflux facilitators, efficient modulation of the ER auxin pool could be achieved and assessed. Consequences of such modulation were quantitatively monitored using microscopy and synthetic biology tools in time-resolved, dose-response assays. We used mathematical modeling to interconnect auxin-mediated cellular responses, nuclear signaling, and potential strength of nuclear auxin fluxes.

The consistency among the quantitative predictions based on the cell expansion data and the auxin-sensor-derived experimental data strongly suggests that a key step in the regulation of cell expansion is the establishment of nuclear auxin levels inside the cell. Furthermore, the data-driven mathematical models of cell expansion (Figures 4) and of the nuclear auxin fluxes (Figure 5) predicted (1) rapid (on a timescale of minutes) establishment of the difference in nuclear auxin signaling between PIN8OX and WT cells after auxin treatment and (2) upon increase of exogenous auxin concentration, receptor occupancy in PIN8OX cells remains lower than in WT. These predictions were confirmed using the ratiometric auxin sensor and led to our key model-driven hypothesis summarized in Figure 7D: the ER-to-nucleus flux is a dominant route for nuclear auxin uptake. We then tested our hypothesis by exploring the effect of PIN5 overexpression on WT and PIN8OX cells. The model provides a consistent explanation for why PIN5 overexpression results in opposing effects, depending on the type of auxin. In particular, the model indicates that ER-to-nucleus fluxes are mediated by a saturable transport mechanism (Figure S8). This strongly implies that there must exist unidentified molecular players mediating auxin flux between the ER and the nucleus (Figure 7D) that remain to be discovered.

Although ER-residing auxin carriers (Barbez et al., 2012; Dal Bosco et al., 2012; Ding et al., 2012; Mravec et al., 2009) and enzymes involved in auxin deconjugation (Bartel and Fink, 1995; Sanchez Carranza et al., 2016) might modulate auxin levels in the ER, the predicted molecular players should be essential in regulating ER-to-nucleus auxin flux strength. Moreover, the difference in the predicted ER-to-nucleus flux strength derived from the cell expansion and early nuclear auxin response models (10-fold versus 46- to 84-fold, respectively) strongly

corroborates the relevance of other auxin-related processes in the regulation of nuclear auxin content. Upstream auxin regulatory processes, which include auxin synthesis and biochemical modifications, transport in and out of cells and within, collectively forming subcellular auxin pools that define auxin-mediated responses of plant cells during development (Moreno-Risueno et al., 2010) and interaction with the environmental stimuli (Kazan, 2013). In this context, and because auxin is a small and mobile molecule with a strong impact on plant cell responses, particularly auxin-mediated transcriptional processes, the ER can be considered a buffer for auxin between the cytosol and the nucleus, while the predicted ER-to-nucleus auxin flux provides the means for tight regulation of auxin interaction with TIR1/AFB-Aux/IAA machinery and downstream responses. We therefore believe our approach provides a basis for integration of these processes and elaboration of more comprehensive models in the future.

Our results are particularly intriguing in light of growing evidence that in plants, the ER is home to several putative hormone transporters, receptors, and enzymes that regulate homeostasis not only of auxin but possibly of cytokinin (Wulfetange, et al., 2011), ethylene (Bisson et al., 2009), jasmonate (Koo, et al., 2014), and other hormones. Therefore, our finding suggests a direct link between ER-based homeostatic mechanisms and nuclear auxin signaling, in which the ER plays the role of the main conduit for nuclear auxin uptake, as well as an important site for hormonal crosstalk.

#### EXPERIMENTAL PROCEDURES

Further details about experimental procedures, mathematical modeling, statistical analysis, and an outline of resources used in this work can be found in [Supplemental Experimental Procedures](#).

#### DATA AND SOFTWARE AVAILABILITY

Code developed as part of this work can be found at [https://gitlab.com/wurssb/ER\\_Controls\\_Nuclear\\_Auxin\\_Uptake](https://gitlab.com/wurssb/ER_Controls_Nuclear_Auxin_Uptake). Further information on this code should be directed to A.D.

#### SUPPLEMENTAL INFORMATION

Supplemental Information includes Supplemental Experimental Procedures, nine figures, and four tables and can be found with this article online at <https://doi.org/10.1016/j.celrep.2018.02.074>.

#### ACKNOWLEDGMENTS

The authors acknowledge Katja Rapp for technical support, Dr. Xin Yu for providing PIN5 cDNA, and Dr. Claude Becker for HTB4-mCherry construct. We thank Prof. Markus Owen for critically reading the manuscript. We gratefully acknowledge the help of Dr. Thorsten Falk for revising the AutoOvuscule code. This work was supported by Bundesministerium für Bildung und Forschung (BMBF SYSBRA, SYSTEC, Microsystems), the Excellence Initiative of the German Federal and State Governments (EXC 294), and the German Research Foundation (DFG SFB746 and INST 39/839,840,841). C.D.B. acknowledges support from Deutsches Zentrum für Luft und Raumfahrt (DLR 50WB1022). F.R. was supported by InKoMBio (SPP1395). A.D. and K.P. were supported by the European Union Framework 6 Program (AUTOSCREEN, LSHG-CT-2007-037897). A.M.M., K.P., and C.F. received support from the BMBF Freiburg Initiative in Systems Biology (FRISYS) (0313921). S.W., M.D.Z., and W.W. were supported by the Initiating and

Networking Fund of the Helmholtz Association within the Helmholtz Initiative on Synthetic Biology (SO-078) and the Alexander von Humboldt Foundation (1141629).

#### AUTHOR CONTRIBUTIONS

Conceptualization, C.F., A.D., C.D.B., A.M.M., and K.P.; Investigation, A.D., C.D.B., F.R., S.B., A.M.M., and C.F.; Formal Analysis, A.M.M., A.D., C.D.B., and C.F.; Methodology & Software, P.C., R.B., O.R., A.D., C.D.B., S.W., M.D.Z., H.H., and R.U.; Resources, W.W., M.D.Z., H.H., R.U., and K.H.; Writing – Original Draft, A.D., A.M.M., C.F., P.C., and C.D.B.; Writing – Review & Editing, A.D., A.M.M., C.F., C.D.B., K.P., K.H., M.D.Z., R.B., and O.R.; Funding Acquisition, A.D., C.F., O.R., and K.P.

#### DECLARATION OF INTERESTS

The authors declare no competing interests.

Received: September 26, 2016

Revised: December 18, 2017

Accepted: February 19, 2018

Published: March 13, 2018

#### REFERENCES

- Abel, S., Nguyen, M.D., and Theologis, A. (1995). The PS-IAA4/5-like family of early auxin-inducible mRNAs in *Arabidopsis thaliana*. *J. Mol. Biol.* *251*, 533–549.
- Barbez, E., Kubeš, M., Rolčík, J., Béziat, C., Pěncík, A., Wang, B., Rosquete, M.R., Zhu, J., Dobrev, P.I., Lee, Y., et al. (2012). A novel putative auxin carrier family regulates intracellular auxin homeostasis in plants. *Nature* *485*, 119–122.
- Bartel, B., and Fink, G.R. (1995). ILR1, an amidohydrolase that releases active indole-3-acetic acid from conjugates. *Science* *268*, 1745–1748.
- Bisson, M.M., Bleckmann, A., Allekotte, S., and Groth, G. (2009). EIN2, the central regulator of ethylene signalling, is localized at the ER membrane where it interacts with the ethylene receptor ETR1. *Biochem. J.* *424*, 1–6.
- Brunoud, G., Wells, D.M., Oliva, M., Larrieu, A., Mirabet, V., Burrow, A.H., Beeckman, T., Kepinski, S., Traas, J., Bennett, M.J., and Vernoux, T. (2012). A novel sensor to map auxin response and distribution at high spatio-temporal resolution. *Nature* *482*, 103–106.
- Calderón Villalobos, L.I.A., Lee, S., De Oliveira, C., Ivetac, A., Brandt, W., Armitage, L., Sheard, L.B., Tan, X., Parry, G., Mao, H., et al. (2012). A combinatorial TIR1/AFB-Aux/IAA co-receptor system for differential sensing of auxin. *Nat. Chem. Biol.* *8*, 477–485.
- Campanoni, P., and Nick, P. (2005). Auxin-dependent cell division and cell elongation. 1-Naphthaleneacetic acid and 2,4-dichlorophenoxyacetic acid activate different pathways. *Plant Physiol.* *137*, 939–948.
- Charpentier, M., and Oldroyd, G.E. (2013). Nuclear calcium signaling in plants. *Plant Physiol.* *163*, 496–503.
- Dal Bosco, C., Dovzhenko, A., Liu, X., Woerner, N., Rensch, T., Eismann, M., Eimer, S., Hegemann, J., Paponov, I.A., Ruperti, B., et al. (2012). The endoplasmic reticulum localized PIN8 is a pollen-specific auxin carrier involved in intracellular auxin homeostasis. *Plant J.* *71*, 860–870.
- Delbarre, A., Muller, P., Imhoff, V., and Guern, J. (1996). Comparison of mechanisms controlling uptake and accumulation of 2,4-dichlorophenoxy acetic acid, naphthalene-1-acetic acid, and indole-3-acetic acid in suspension-cultured tobacco cells. *Planta* *198*, 532–541.
- Dharmasiri, N., Dharmasiri, S., and Estelle, M. (2005). The F-box protein TIR1 is an auxin receptor. *Nature* *435*, 441–445.
- Ding, Z., Wang, B., Moreno, I., Dupláková, N., Simon, S., Carraro, N., Reemmer, J., Pěncík, A., Chen, X., Tejos, R., et al. (2012). ER-localized auxin transporter PIN8 regulates auxin homeostasis and male gametophyte development in *Arabidopsis*. *Nat. Commun.* *3*, 941.

- Dunlap, J.R., Kresovich, S., and McGee, R.E. (1986). The effect of salt concentration on auxin stability in culture media. *Plant Physiol.* *81*, 934–936.
- Feraru, E., Feraru, M.I., Kleine-Vehn, J., Martinière, A., Mouille, G., Vanneste, S., Vernhettes, S., Runions, J., and Friml, J. (2011). PIN polarity maintenance by the cell wall in *Arabidopsis*. *Curr. Biol.* *21*, 338–343.
- Freire Rios, A., Yoshida, S., and Weijers, D. (2014). Auxin regulation of embryo development. In *Auxin and Its Role in Plant Development*, E. Zazimalova, J. Petrasek, and E. Benkova, eds. (Springer-Verlag), pp. 171–189.
- Ganguly, A., Lee, S.H., Cho, M., Lee, O.R., Yoo, H., and Cho, H.T. (2010). Differential auxin-transporting activities of PIN-FORMED proteins in *Arabidopsis* root hair cells. *Plant Physiol.* *153*, 1046–1061.
- Görllich, D., and Kutay, U. (1999). Transport between the cell nucleus and the cytoplasm. *Annu. Rev. Cell Dev. Biol.* *15*, 607–660.
- Hayashi, K., Nakamura, S., Fukunaga, S., Nishimura, T., Jenness, M.K., Murphy, A.S., Motose, H., Nozaki, H., Furutani, M., and Aoyama, T. (2014). Auxin transport sites are visualized in planta using fluorescent auxin analogs. *Proc. Natl. Acad. Sci. USA* *111*, 11557–11562.
- Kazan, K. (2013). Auxin and the integration of environmental signals into plant root development. *Ann. Bot.* *112*, 1655–1665.
- Kepinski, S., and Leyser, O. (2005). The *Arabidopsis* F-box protein TIR1 is an auxin receptor. *Nature* *435*, 446–451.
- Koo, A.J., Thireault, C., Zemelis, S., Poudel, A.N., Zhang, T., Kitaoka, N., Brandizzi, F., Matsuura, H., and Howe, G.A. (2014). Endoplasmic reticulum-associated inactivation of the hormone jasmonoyl-L-isoleucine by multiple members of the cytochrome P450 94 family in *Arabidopsis*. *J. Biol. Chem.* *289*, 29728–29738.
- Lieleg, O., and Ribbeck, K. (2011). Biological hydrogels as selective diffusion barriers. *Trends Cell Biol.* *21*, 543–551.
- Meier, I., and Brkljacic, J. (2010). The *Arabidopsis* nuclear pore and nuclear envelope. *Arabidopsis Book* *8*, e0139.
- Moreno-Risueno, M.A., Van Norman, J.M., Moreno, A., Zhang, J., Ahnert, S.E., and Benfey, P.N. (2010). Oscillating gene expression determines competence for periodic *Arabidopsis* root branching. *Science* *329*, 1306–1311.
- Mravec, J., Skúpa, P., Bailly, A., Hoyerová, K., Krecek, P., Bielach, A., Petrásek, J., Zhang, J., Gaykova, V., Stierhof, Y.D., et al. (2009). Subcellular homeostasis of phytohormone auxin is mediated by the ER-localized PIN5 transporter. *Nature* *459*, 1136–1140.
- Naseem, M., Kaldorf, M., and Dandekar, T. (2015). The nexus between growth and defence signalling: auxin and cytokinin modulate plant immune response pathways. *J. Exp. Bot.* *66*, 4885–4896.
- Oparka, K.J., Duckett, C.M., Prior, D.A.M., and Fisher, D.B. (1994). Real-time imaging of phloem unloading in the root tip of *Arabidopsis*. *Plant J.* *6*, 759–766.
- Salehin, M., Bagchi, R., and Estelle, M. (2015). SCFTIR1/AFB-based auxin perception: mechanism and role in plant growth and development. *Plant Cell* *27*, 9–19.
- Sanchez Carranza, A.P., Singh, A., Steinberger, K., Panigrahi, K., Palme, K., Dovzhenko, A., and Dal Bosco, C. (2016). Hydrolases of the ILR1-like family of *Arabidopsis thaliana* modulate auxin response by regulating auxin homeostasis in the endoplasmic reticulum. *Sci. Rep.* *6*, 24212.
- Steffens, B., and Lüthen, H. (2000). New methods to analyse auxin-induced growth II: The swelling reaction of protoplasts—a model system for the analysis of auxin signal transduction? *Plant Growth Regul.* *32*, 115–122.
- Steffens, B., Feckler, C., Palme, K., Christian, M., Böttger, M., and Lüthen, H. (2001). The auxin signal for protoplast swelling is perceived by extracellular ABP1. *Plant J.* *27*, 591–599.
- Steinacher, A., Leyser, O., and Clayton, R.H. (2012). A computational model of auxin and pH dynamics in a single plant cell. *J. Theor. Biol.* *296*, 84–94.
- Steinwand, B.J., Xu, S., Polko, J.K., Doctor, S.M., Westafer, M., and Kieber, J.J. (2014). Alterations in auxin homeostasis suppress defects in cell wall function. *PLoS ONE* *9*, e98193.
- Tan, X., Calderon-Villalobos, L.I., Sharon, M., Zheng, C., Robinson, C.V., Estelle, M., and Zheng, N. (2007). Mechanism of auxin perception by the TIR1 ubiquitin ligase. *Nature* *446*, 640–645.
- Taylor-Teeple, M., Lanctot, A., and Nemhauser, J.L. (2016). As above, so below: auxin's role in lateral organ development. *Dev. Biol.* *419*, 156–164.
- Wang, R., and Estelle, M. (2014). Diversity and specificity: auxin perception and signaling through the TIR1/AFB pathway. *Curr. Opin. Plant Biol.* *21*, 51–58.
- Wei, X., Henke, V.G., Strübing, C., Brown, E.B., and Clapham, D.E. (2003). Real-time imaging of nuclear permeation by EGFP in single intact cells. *Biophys. J.* *84*, 1317–1327.
- Wend, S., Dal Bosco, C., Kämpf, M.M., Ren, F., Palme, K., Weber, W., Dovzhenko, A., and Zurbriggen, M.D. (2013). A quantitative ratiometric sensor for time-resolved analysis of auxin dynamics. *Sci. Rep.* *3*, 2052.
- Winicur, Z.M., Zhang, G.F., and Staehelin, L.A. (1998). Auxin deprivation induces synchronous Golgi differentiation in suspension-cultured tobacco BY-2 cells. *Plant Physiol.* *117*, 501–513.
- Wu, M.F., Yamaguchi, N., Xiao, J., Bargmann, B., Estelle, M., Sang, Y., and Wagner, D. (2015). Auxin-regulated chromatin switch directs acquisition of flower primordium founder fate. *eLife* *4*, e09269.
- Wulfetange, K., Lomin, S.N., Romanov, G.A., Stolz, A., Heyl, A., and Schmölling, T. (2011). The cytokinin receptors of *Arabidopsis* are located mainly to the endoplasmic reticulum. *Plant Physiol.* *156*, 1808–1818.
- Yoo, S.D., Cho, Y.H., and Sheen, J. (2007). *Arabidopsis* mesophyll protoplasts: a versatile cell system for transient gene expression analysis. *Nat. Protoc.* *2*, 1565–1572.